UNIVERSITY of BARCELONA

Master in Quantum Science and Technology

SiPM-Based Detection Methods for Evaluating Single-Photon Sources

Taiki Aritomi

Supervisor : Daniel Alberto Guberman and Raul Lahoz Sanz

Course 2024 2025

SiPM-Based Detection Methods for Evaluating Single-Photon Sources

Taiki Aritomi

Supervised by: Daniel Alberto Guberman Raul Lahoz Sanz

Facultad de Física UB (ICCUB), 08028 Barcelona
7 July 2025

Silicon Photomultipliers (SiPMs) are emerging as promising photon detectors in quantum optics due to their high photon detection efficiency(PDE), excellent timing resolution, and photon-number resolution capabilities. Their potential to replace conventional single-photon detectors makes them attractive for applications in many quantum technologies.

In this study, I first performed a detailed characterization of SiPMs to assess their performance parameters, including dark count rate(DCR) and single-photon time resolution(SPTR). I then implemented these SiPMs in an existing experimental setup designed to evaluate single-photon sources (SPS), in order to test their feasibility for use in quantum-optical experiments.

Although challenges arose, including alignment limitations and high dark count rates inherent to SiPMs, the system was able to register photon count rate changes under various SPS conditions. While anti-bunching was not observed, the results provide practical insights into the integration of SiPMs in single-photon-level experiments and outline conditions necessary for future successful implementation.

Acknowledgements

I am deeply grateful to my supervisor, Professor Daniel Alberto Guberman, and Raul Lahoz Sanz, for their insightful feedback, continuous encouragement, and invaluable support throughout this research. I would also like to sincerely thank David, whose guidance was essential in learning how to properly handle and operate the SiPM devices used in this thesis. I am especially thankful to Ms. Coral Becerra Gómez and Professor Albert Figuerola for providing the nanorod-shaped CdSe-CdS core-shell quantum dots, which played a crucial role as single photon sources in the experimental part of this work. My gratitude also extends to Professors Bruno Julia Diaz and José María Gómez Cama, as well as all the faculty members, for their helpful discussions and valuable guidance during the weekly group meetings.

This study was supported by MCIN with funding from European Union NextGenerationEU(PRTR-C17.I1) and by Generalitat de Catalunya. We acknowledge funding from Grants PID2023-147475NB-I00 and CEX2024-001451-M financed by MCIN/AEI/10.13039/501100011033 and Grants 2021SGR01095, and 2021SGR01108 by Generalitat de Catalunya. This project

Taiki Aritomi: taritoar28@alumnes.ub.edu

has received funding from the European Union's Digital Europe Programme under grant agreement no. 101084035.

Contents

This thesis is organized as follows: In Sec. 1, I present a brief introduction of the advantages and growing expectations surrounding Silicon Photonmultipliers(SiPMs), along with the current state of research in this area. Sec. 2 outlines the motivations for this work. In Sec. 3, I set the objectives of this study. In Sec. 4, I explain the fundamentals of SiPMs to support understanding of the later chapters. In Sec. 5, I performed the deep characterization of two sizes of SiPMs. Sec. 6 describes the experimental setup and experimental conditions used to evaluate the performance of a single-photon source (SPS). In Sec. 7, I compare the experimental results obtained using SiPMs and SPADs, and discuss both the advantages and limitations of SiPMs in this context. Finally, Sec. 8 summarizes the conclusions and proposes future directions for research.

1 Introduction

The Silicon Photomultiplier (SiPM) has emerged as a next-generation photon detector gaining increasing attention in the field of quantum technologies[AG19]. Its strengths can be broadly categorized into three main aspects.

First, high sensitivity: SiPMs are composed of an array of Single-Photon Avalanche Diodes (SPADs) connected in parallel[ons21], enabling them to maintain the same high sensitivity as SPADs, which are capable of generating clear signals from even a single photon. This property makes SiPMs highly suitable for applications in quantum sensing, light communication[ASA+20], medical imaging and so on.

Second, photon-number resolution: Unlike conventional SPADs, SiPMs can distinguish between different numbers of incident photons, an essential feature for applications in quantum communication, quantum random number generation(QRNG [AJW+23]) and so on where precise photon number control is required.

Third, SiPMs exhibit excellent time resolution due to their SPAD-array structure, which minimizes dead time. As a result, they can record photon arrival times with precision on the order of tens of picoseconds, which is crucial in time-correlated measurements. Thanks to this advantage, SiPMs are increasingly expected to play key roles in applications such as LiDAR [RA13] and medical imaging, particularly in positron emission tomography (PET) [BDB19].

2 Motivation

In this thesis, I apply SiPMs to a pre-existing experimental system built to characterize a Single Photon Source(SPS), in order to demonstrate their applicability as photon detectors in quantum experiments. The demand for reliable SPSs continues to grow, as the ability to generate true single photons underpins various emerging quantum technologies—including quantum key distribution[BB14], photonic quantum computing[KE01], and fundamental quantum optics experiments.

While previous SPS characterization studies have primarily used SPAD-based detectors, implementing SiPMs may offer improvements in timing resolution and photon-number discrimination. Therefore, this work aims to serve both as an early demonstration of SiPM integration in quantum optical experiments and as a contribution to improving the methodology of SPS evaluation.

3 Objectives

The long term goal of this thesis is to study the feasibility of using SiPMs in quantum communications.

As a first step, this thesis aims to:

- Characterize the baseline performance of SiPMs (dark count rate, time resolution, photon response),

- Implement SiPMs in a quantum optics setup for SPS evaluation,
- Experimentally investigate whether anti-bunching can be observed using SiPMs, despite their relatively high dark count rate.

4 Fundamentals of SiPMs

4.1 Basic Principle

A silicon photomultiplier (SiPM) is a densely integrated array of small, independent sensors known as single-photon avalanche diodes (SPADs). For example, the SiPM which I used consisted of around 600 SPADs. As a result, the detection mechanism of a SiPM is fundamentally the same as that of a SPAD. SPADs detect incident photons by converting optical energy into an electrical signal through the process of avalanche multiplication. The detection mechanism is explained in detail below. Silicon is a suitable photodetector material because it efficiently absorbs a wide range of optical wavelengths. When a photon is absorbed by the silicon layer, it generates an electron–hole pair. Under a strong electric field applied to the SiPM, the generated carriers (electrons and holes) are accelerated and can acquire sufficient kinetic energy to ionize other atoms in the lattice. This leads to the creation of additional electron–hole pairs in a chain reaction, known as avalanche breakdown. This multiplication process results in a macroscopic current pulse that can be measured as an analog signal. Notably, even a single photon can trigger a significant current, giving SiPMs their high sensitivity.

Moreover, since SiPMs are an array of SPADs (also known as microcells) connected in parallel, the output signal is proportional to the number of fired SPADs, which is often proportional to the number of detected photons.

4.2 Important Indicators

There are three characteristics of SiPMs that are particularly relevant for this thesis: photon detection efficiency (PDE), dark count rate (DCR), and optical crosstalk. This section describes the characteristics and significance of each.

Photon Detection Efficiency (PDE) refers to the ratio of detected photons to the total number of incident photons, in short this is the measure of the probability of detecting an incident photon. PDE is primarily determined by three factors: quantum efficiency (QE), fill factor (FF), and the probability of triggering a successful avalanche (which depends on the overvoltage). The influence of overvoltage is discussed in detail in Sec. 4.3. Quantum efficiency is the probability that an incident photon generates an electron–hole pair. It depends on the semiconductor material and is not easily tunable. Fill factor represents the proportion of the active area (photon-sensitive region) relative to the total device area.

Dark Count Rate (DCR) refers to the rate of events caused by thermally generated carriers. At room temperature, some electrons can be thermally excited and subsequently accelerated by the applied electric field, potentially triggering avalanche breakdown. As a result, DCR strongly depends on both temperature and overvoltage.

Optical Crosstalk is another form of noise. During avalanche multiplication in one SPAD cell, secondary photons may be emitted. These photons can travel to neighboring SPADs and trigger avalanches there, causing a single-photon event to be falsely registered as multiple detections. Crosstalk can also be enhanced by thermally generated photons, and since DCR increases with overvoltage, crosstalk is also indirectly affected by it. In addition, fill factor influences crosstalk: the denser the SPAD array, the higher the probability that secondary photons will reach adjacent cells.

4.3 Overvoltage

Overvoltage is a critical parameter that influences all three key performance indicators discussed above: photon detection efficiency (PDE), dark count rate (DCR), and optical crosstalk. It refers to the amount of voltage applied above the breakdown voltage of the SiPM. The breakdown voltage is the minimum voltage at which avalanche breakdown can occur. To operate a SiPM effectively, the applied bias voltage must exceed this threshold.

Increasing the overvoltage enhances the electric field strength across the SPADs, which has several consequences. Firstly, PDE increases because carriers (electrons and holes) gain more energy and are more likely to initiate avalanche multiplication when a photon is absorbed. Secondly, DCR also increases, as thermally generated carriers are more likely to trigger false avalanches under a stronger electric field. Finally, optical crosstalk becomes more prominent. This occurs for two main reasons: (1) A larger avalanche current produces more secondary photons, which may reach and activate neighboring SPADs; (2) An increased DCR raises the chance that thermally generated events themselves cause additional crosstalk.

In summary, while increasing overvoltage can improve PDE, it also exacerbates noise sources such as DCR and crosstalk. Therefore, selecting an optimal overvoltage is essential to balance sensitivity and signal integrity in SiPM-based detection systems.

5 Detailed Characterization of Each SiPM Size

This section describes the methods and results of the characterization for each SiPM size: $3 \times 3mm^2$ and $1 \times 1mm^2$ SiPMs.

5.1 Characterization of SiPM (3×3 mm^2)

As a first step, I performed a characterization of a single SiPM chip with an active area of 3×3 mm^2.

5.1.1 Experimental Setup

The experimental setup is shown in Fig 1. Photons are emitted from a pulsed laser and arrive at the surface of the SiPM and SiPM outputs a macroscopic current pulse. The analog output from the SiPM is amplified and shaped by quatom-made electronics and digitized by an oscilloscope, enabling the acquisition of both the arrival time and the amplitude of each photon detection event.

In this experiment, an external trigger was used to define the time window of 300 ns for each event. A total of 40,000 waveforms were recorded, each containing timing and amplitude information. To investigate the effect of overvoltage, the bias voltage was varied from 36V to 45V in 3V increments. Additionally, measurements were taken both with the laser turned ON and OFF, to distinguish between real photon events and noises.

5.1.2 Pulse amplitude histogram

For each waveform I looked for the maximum amplitude within a time window of 100 ns around the expected arrival time of the laser pulses. These peak values were compiled into a histogram as shown in Fig 2.

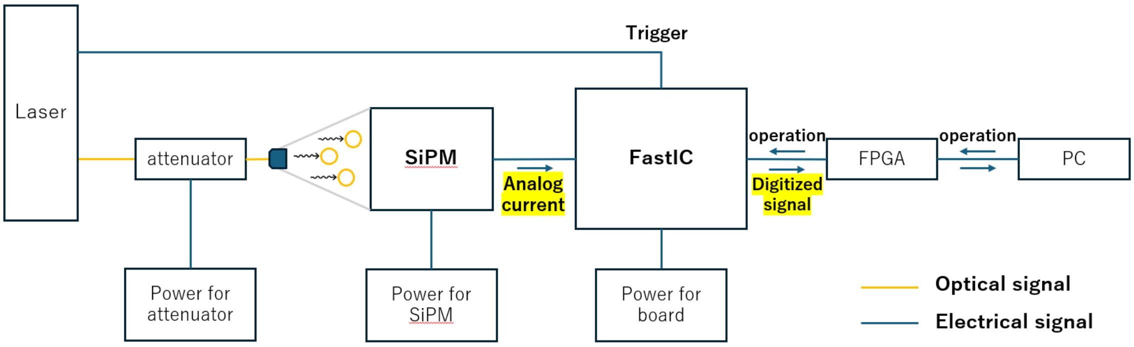

Figure 1: The setup to characterize 3 by 3 SiPM

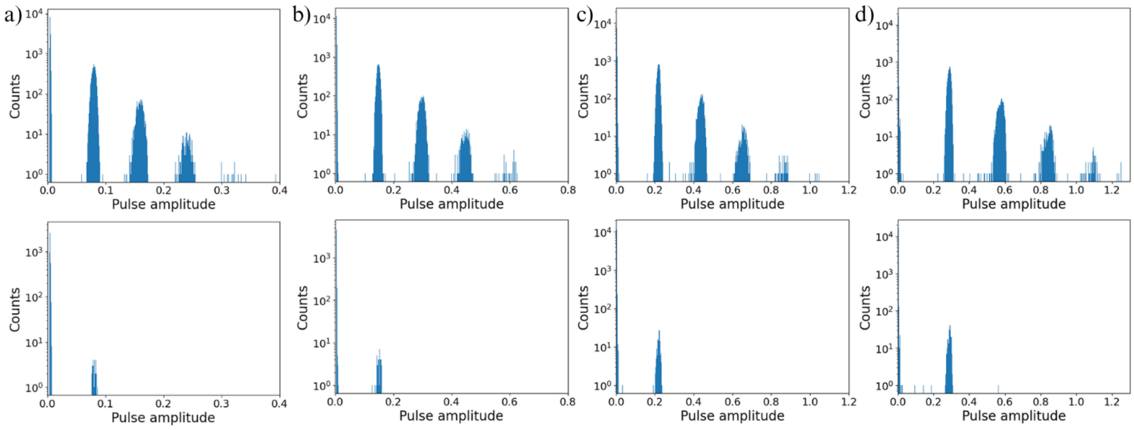

Figure 2: Energy width histogram of all condition, upper figures are with laser on and lowers are with laser off. Applied voltages are a)36V, b)39V, c)42V, d)45V.

1. Presence of dark counts
   By comparing the histograms with the laser on and off, it is evident that the spectra under laser-on conditions exhibit multiple peaks, whereas those under laser-off conditions show only two distinct peaks. These two peaks correspond to 0-photon and 1-photon events. Since no external photons are present in the laser is off, the 1-photon events can be attributed to dark counts caused by thermally generated carriers.

2. Effect of overvoltage on peak separation
   Examining the laser-on histograms for different bias voltages (45V, 42V, 39V, and 36V), we observe that the spacing between adjacent peaks increases with overvoltage. This occurs because a higher overvoltage (ΔV) enhances the avalanche gain, resulting in a larger output current for each photon detection. Since the total output signal of the SiPM is a superposition of signals from individual SPADs, an increase in ΔV raises the amplitude of each peak, thereby widening the peak-to-peak separation.

5.1.3 Mean number of detected photons

In this section, we estimate the mean number of triggered SPADs per event both from photons and dark counts based on the Poisson distribution. The detail theory of it is written in Appendix. The mean number of photons is obtained by following equation[OHM+06]:

$$\begin{aligned} N_{ph} &= N_{ph+DC} - N_{DC} \\ &= -ln\frac{N_0^{ON}}{N_{tot}} + ln\frac{N_0^{OFF}}{N_{tot}} \\ &= ln\frac{N_0^{OFF}}{N_0^{ON}} \end{aligned} \tag{1}$$

Where:N_{tot} is the total number of laser triggers (events), N_0 is the number of events in which no signal above threshold was detected, and N_{ph}, N_{ph+DC}, N_{DC} are the mean number of photon, photon and Dark count and Dark count. The uncertainty in N_{ph} is given by:

$$\Delta N_{ph} = \sqrt{\left(\frac{\Delta N_0^{ON}}{N_0^{ON}}\right)^2 + \left(\frac{\Delta N_0^{OFF}}{N_0^{OFF}}\right)^2} \tag{2}$$

Based on the above equation, the data were processed, and the results are summarized in the Table 1.

Table 1: The mean number of detected photons

	N_{ph}	ΔN_{ph}
45V	0.501	8.31×10^{-3}
42V	0.476	8.21×10^{-3}
39V	0.467	8.15×10^{-3}
36V	0.414	7.98×10^{-3}

This expression allows us to estimate the mean number of detected photons per pulse, independent of dark counts and crosstalk, under the assumption that both types of events follow Poisson statistics. Fig 3 shows N_{ph} versus bias voltage.

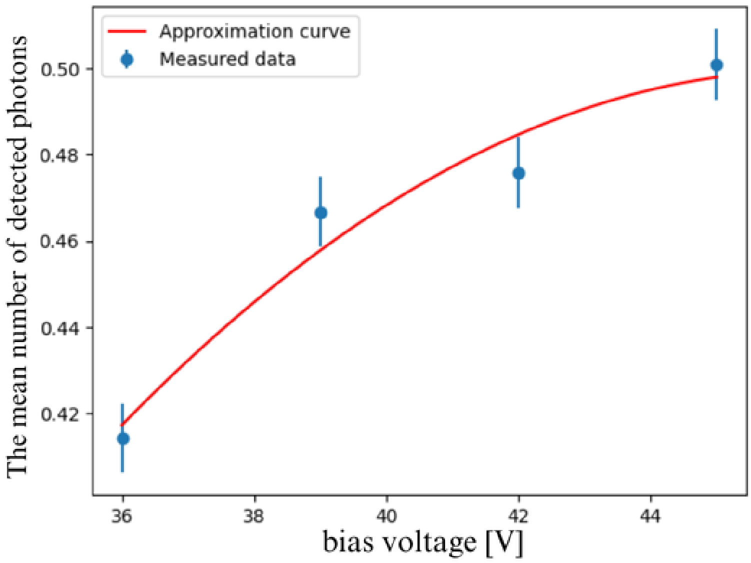

Figure 3: The plot of N_{ph} vs overvoltage

The mean number of photons increases with overvoltage. The slope of this trend decreases for higher overvoltages until it reaches a plateau. This is expected since N_{ph} is proportional to the SiPM PDE. PDE increases with overvoltage because the probabilty of triggering a succesful avalanche increases with the strength of the electric field. But this probability saturates at high overvoltages[ons21].

5.1.4 Dark count rate

The Dark Count Rate (DCR) refers to the number of thermally induced detection events per second and is expressed in hertz (Hz). This is conceptually different from N_{DC}, which represents the mean number of dark counts per trigger (or per measurement event). To convert N_{DC} into a rate, it is divided by the time window used for a single measurement (see equation 3). In our experimental setup, the time window used for each waveform was precisely 319.688 ns.

$$DCR = \frac{N_{DC}}{timewindow \times 10^{-9}} \tag{3}$$

Additionaly, considering uncertainty is also necessary in this case, and the equation can be described as equation 4.

$$\Delta DCR = \sqrt{\frac{\Delta N_{DC}}{timewindow * 10^{-9}}} \tag{4}$$

The Table 2 summarizes the calculated DCR values for different applied bias voltages:

To investigate the relationship between DCR and overvoltage, we plotted the DCR values as a function of overvoltage (ΔV) and performed a linear regression. This result shows that DCR increases approximately linearly with overvoltage, consistent with theoretical expectations. The plot is shown in Fig 4.

Table 2: Calculated DCR at each bias voltage

Voltage[V]	DCR	ΔDCR
45V	1.26×10^5	4.73×10^2
42V	9.96×10^4	4.72×10^3
39V	7.21×10^4	4.72×10^2
36V	4.03×10^4	4.71×10^2

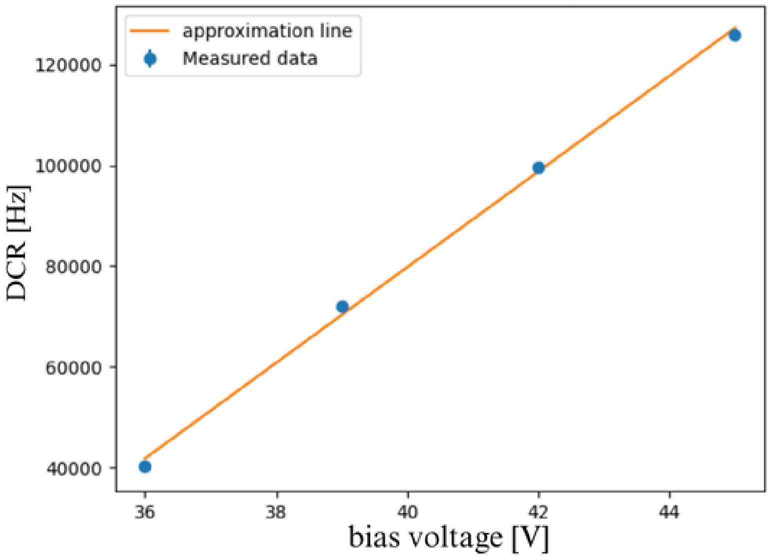

Figure 4: Correlation between Dark Count Rate and bias voltage

5.1.5 Crosstalk probability

The crosstalk probability represents the likelihood that an optical crosstalk event occurs when a photon detection triggers an avalanche in one SPAD cell and subsequently induces avalanches in neighboring cells. It is calculated using the equation 5.

$$P_{crosstalk} = \frac{N_{\geq 2ph}}{N_{\geq 1ph}} \tag{5}$$

Where $N_{\geq 2\ ph}$ is the number of events in which two or more SPAD cells fire simultaneously, and $N_{\geq 1\ ph}$ is the number of events in which at least one SPAD cell fires. These values are extracted by analyzing the pulse amplitude histograms: each peak corresponds to a distinct number of fired SPAD cells (photoelectrons), therefore by applying suitable amplitude thresholds, the desired event counts can be reliably obtained.

The results are summarized in Table 3 and plotted in Fig. 5. As can be observed, the crosstalk probability increases with the applied bias voltage and then begins to saturate. This behavior is expected, as higher overvoltages enhance the gain and light emission during avalanche events, increasing the probability of crosstalk. However, as seen also in Sec. 5.1.3, this effect levels off at higher voltages due to saturation in triggering probability.

Bias voltage [V]	Crosstalk probability [%]
45	6.97×10^{-3}
42	5.07×10^{-3}
39	6.34×10^{-4}

Table 3: Crosstalk probability of each bias voltage

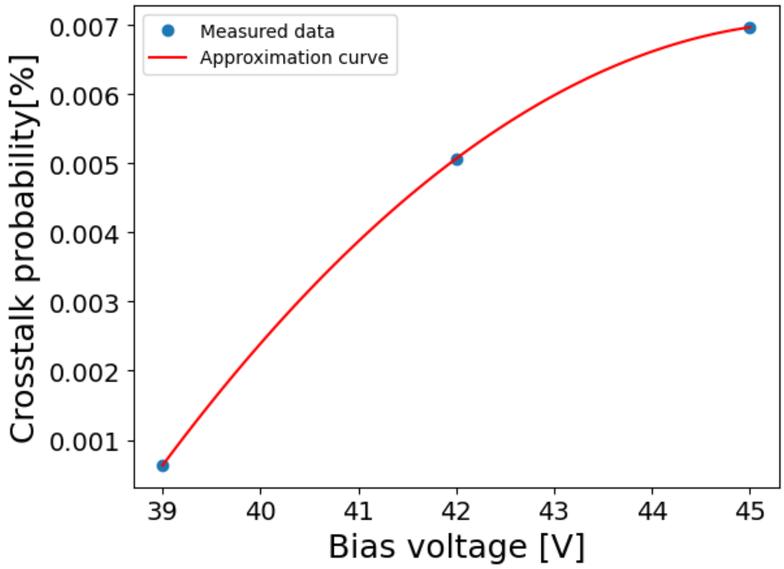

Figure 5: Crosstalk probability versus bias voltage

5.2 Compact SiPMs ($1 \times 1mm^2 \times 2$ units) Evaluation

In the previous section, it was found that the $3 \times 3mm^2$ SiPM exhibited a dark count rate (DCR) that was too high for reliable SPS evaluation. Therefore, in this section, we introduce and evaluate a more compact $1 \times 1mm^2$ SiPM, which offers a lower DCR and is expected to perform better under such conditions.

5.2.1 Experimental Setup and condition

In this experiment, the only change to the previous setup was the replacement of the SiPM array with two $1 \times 1mm^2$ SiPMs; all other components remained the same. The experimental procedure was carried out in three steps under the conditions summarized in Table 4. First, we operated the system in external trigger mode to calculate the single-photon time resolution(SPTR). Next, we switched to internal trigger mode to measure the count rate under conditions similar to SPS evaluation. Finally, the laser was set to a pulsed at 100 kHz to verify the functionality of the delay histogram processing code developed in this study.

OverVoltage[V]	Laser	trigger	objective
42.5	ON	external	Calculate SPTR
42.5	OFF	internal	Check Count Rate
42.5	ON(100kHz pulse mode)	internal	Check the delay histogram code

Table 4: The experimental condition

5.2.2 Performance Evaluation

The results of the SPTR and DCR measurements are presented in Fig 6a) to c). As expected, the DCR of each channel is around 6×10^4 Hz. It was reduced to approximately one-ninth of that of the $3 \times 3mm^2$ SiPM.

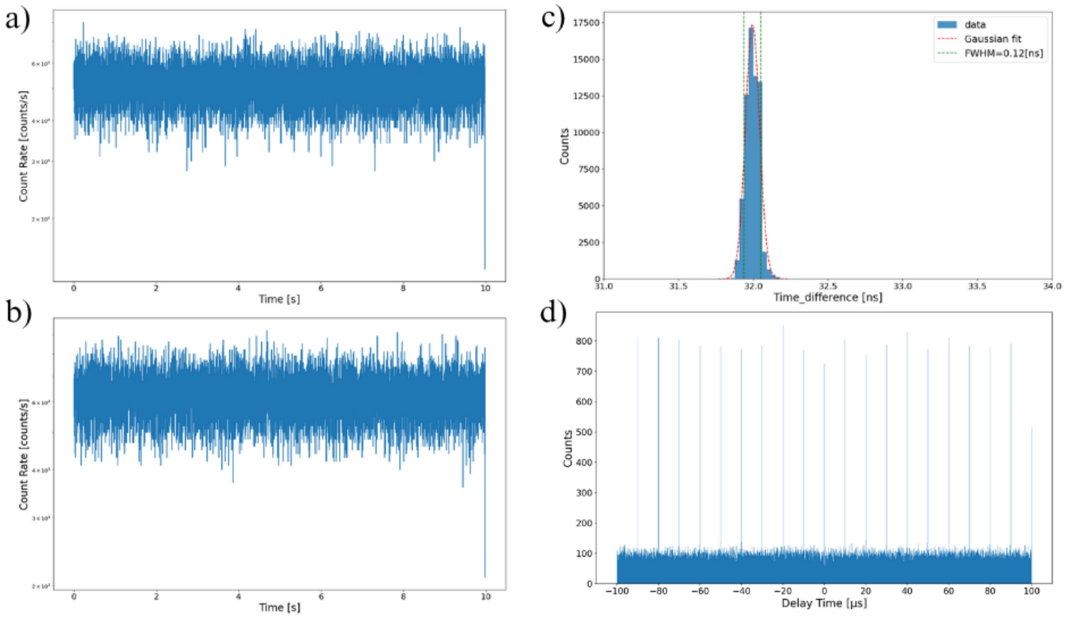

Figure 6: The results with $1 \times 1mm^2$ SiPMs. a)The count rate of Channel 0 and b) Channel 3. c)The SPTR. d)The delay histogram with 100kHz pulse laser.

Secondly, we explain the method used to generate the delay histogram and present the results. In this analysis, for each detection event from ASIC 0, the code calculates the time differences between that event and all detection events recorded by ASIC 1. This comparison continues until the time difference exceeds a preset threshold: in this experiment, $\pm 100\mu s$. The time differences that fall within this range are recorded to create the delay histogram.

For this measurement, the laser was set to pulse mode at 100 kHz, meaning photon arrivals were expected at 10 μs intervals. The result is Fig 6.d). As predicted, the resulting histogram showed clear periodic peaks spaced approximately 10 μs, confirming that the analysis code worked correctly.

6 Evaluation of Single-Photon Source using SiPM

In this chapter, we discuss again the characteristics and advantages of the SiPM, which has been newly introduced in this thesis for the evaluation of single-photon sources (SPS). In the previous chapters, we conducted several baseline experiments to check the performance of the SiPM. While the results revealed some limitations, such as a high dark count rate (DCR), they also highlighted key advantages such as superior time resolution (SPTR).

I begin by comparing the SiPM[Model: NUV-HD-MT 40µm[Gol23]] with the previously used detector in our laboratory, the Single-Photon Avalanche Diode (SPAD) [Model: SPCM-AQ4C[exc20]], based on key performance indicators. This comparison clarifies the potential benefits and challenges of employing SiPMs for SPS evaluation. Following that, we outline the experimental setup used in this study, along with the objectives and specific conditions of each experiment.

6.1 Advantages and limitations

As shown in Table 5, the most significant advantage is time resolution, expressed as SPTR (Single-Photon Time Resolution). SiPMs achieve an SPTR of approximately 80–100 ps, which is about six times better that the SPTR of the SPADs used before in the same experiment. Since the evaluation of SPSs involves analyzing the time difference between photon detection events, time resolution becomes a crucial factor. Therefore, this improvement provides strong justification for adopting SiPMs in this research. Additionally, SiPMs offer a larger active detection area, allowing them to collect and detect more photons than SPADs. Although the photon detection efficiency (PDE) of SiPMs may be lower on the datasheet, their larger area gives them a potential advantage in overall photon collection efficiency.

On the other hand, the dark count rate (DCR) poses a significant challenge. The DCR observed during our experiments was found to be over 100 times greater than that of SPADs. This is because a single SiPM is composed of many SPAD microcells connected in parallel, and its total DCR is effectively the sum of the dark counts from each of these individual units. As a result, the higher DCR increases the risk that true photon signals from the SPS are buried in noise. To solve this issue, longer integration times are required to statistically extract features such as photon anti-bunching. Moreover, the SiPMs used in this thesis are optimized for detection near 410 nm, while the actual emission spectrum of the SPS is around 620 nm. This mismatch further reduces the effective PDE compared to SPADs.

In summary, SiPMs offer significantly improved time resolution, making them well-suited for high-precision SPS evaluation. However, their higher DCR and wavelength mismatch necessitates longer measurement times. This trade-off is a key consideration for future system design and experimental planning.

Indicator	SiPMs	SPADs
PDE for 620 nm	20 %	45 to 60 %
SPTR	80 to 100 ps	600 ps
DCR	40 to 100 kHz	0.5 kHz
Active Area	1 mm^2	0.025 mm^2

Table 5: The differences between main indicators between SiPMs and SPADs

6.2 Experimental Setup

The overall experimental setup is illustrated in Fig 7. It consists of two main components: the photon generation module and the photon detection module.

6.2.1 Photon Generation Module

In the generation part, a nanorod-based single-photon source (SPS)[Sen17] is used. This module is based on a previous setup, and its detailed design and characterization are beyond the scope of this thesis. We therefore focus on the detection part, which is the central contribution of this work.

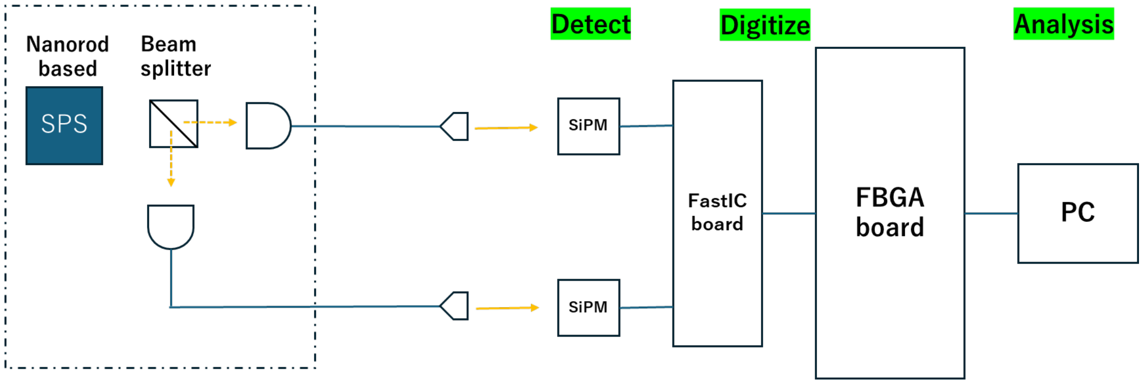

Figure 7: The setup overview

6.2.2 Photon Detection Module (New SiPM-based setup)

In the detection part, the process consists of the following steps:

1. Beam Splitting
   The photons emitted by the SPS are split into two spatially separated paths using a beam splitter.

2. Collection and Coupling
   Each beam is collected and then coupled into an optical fiber.

3. Photon Detection and Digitization
   We set fibers as close as possible to SiPM to increase the photon flux reaching the SiPMs. The photons are detected by two SiPMs (Silicon Photomultipliers). The resulting analog signals are sent to a custom FastIC board[MGM+25] for amplification and digitization. Finally, the digitized data are transferred to a PC for storage and analysis.

This SiPM-based detection system was newly designed and assembled as part of this thesis project.

6.3 Data Acquisition and Processing Method

In this section, we explain the changes in experimental conditions and data acquisition methods used for the evaluation of a single-photon source (SPS). In particular, we focus on the stepwise strategy used to ensure reliable photon detection by the SiPM, and the rationale behind the measurement time settings.

First, to confirm that the SiPMs were properly detecting photons, we observed changes in count rates between SPS ON and OFF states while gradually decreasing the number of nanorod spots. We began with a bunch of spots to ensure a sufficiently high photon emission rate. This was necessary because the SiPMs used in this experiment have a significantly high dark count rate (DCR), which could cause true photon signals to be buried in noise which makes it difficult to determine whether the detectors were functioning properly. The conditions used in this step are summarized in the Table 6.

After confirming proper photon detection, we moved on to the next phase: extending the measurement time. The purpose of this was to statistically average out the effects of DCR and to enhance the visibility of quantum optical features such as photon anti-bunching. Specifically, we set the measurement time to 10 minutes for a bunch of spots

number of spots	measurement time[s]	Laser
bunch of spots	60	ON and OFF
1 spot	60	ON and OFF

Table 6: The measurement condition

and 60 minutes for a single spot. The justification for these time settings is discussed in detail in Section 10, along with the corresponding count rate results.

7 Experimental Results and Discussion

7.1 Comparative results obtained with SPADs

Before presenting the results obtained with SiPMs, this section introduces the comparative data acquired using SPADs in a previous setup. The experimental configuration was nearly identical to the one shown in Fig 7, except that SPADs and a Time-Tagger were used instead of SiPMs, FastIC board, and FPGA board. The measurement conditions remained same.

Figures 8.a) and b) show the time series of count rates for the "bunch of spots" and "single spot" conditions. Table 7 summarizes the count rates for each channel. As seen in the plots, the count rates fluctuate over time due to the blinking behavior of the nanorods.

Number of spot	Channel 1 [Hz]	Channel 2 [Hz]
Bunch of spots	1.73×10^5	1.32×10^5
Single spot	5.67×10^4	4.83×10^4

Table 7: The count rates of each condition

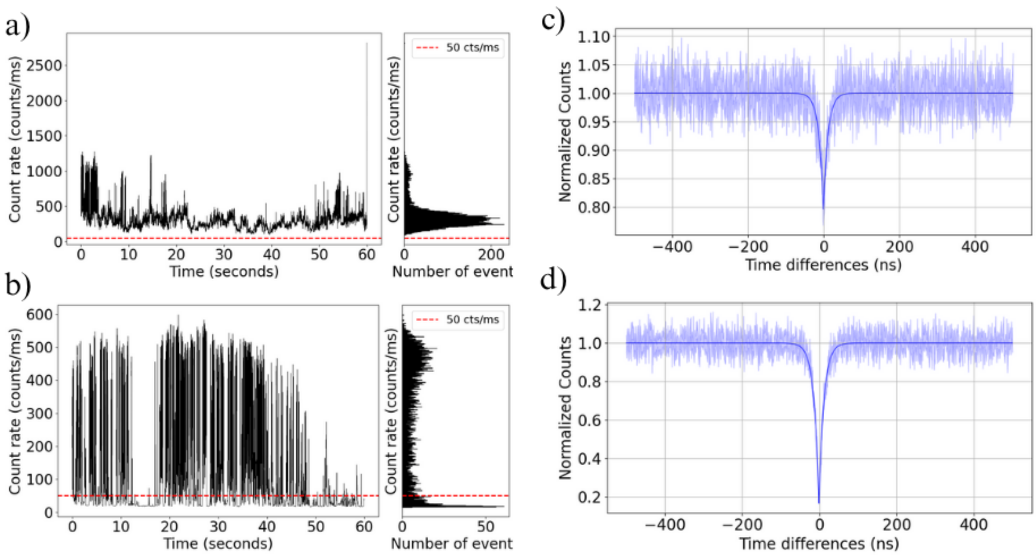

Figure 8: The reference results of SPS with SPADs. a)The count rate of bunch os spots with SPADs. b)The count rate of single spot with SPADs. c)Normalized delay histogram of bunch of spots with SPADs. d)Normalized delay histogram of single spot with SPADs.

Next, the delay histograms for both conditions are shown in figures 8.c) and d). These histograms are normalized using the equation 6.

$$f_{norm}(\tau) = 1 - be^{-\frac{|\tau-\tau_0|}{\tau_x}} \tag{6}$$

Where b represents the depth of anti-bunching dip, τ_0 is the center of the dip, and τ_x is the decay lifetime. In Fig 8.d), the dip falls below 0.5, indicating that the source emits nearly one photon at a time, as expected for a good single-photon source. On the other hand, the dip in Fig 8.c) doesn't drop below 0.5. This is due to multiple nanorods emitting single photon simultaneously, leading to higher coincidence counts. Nonetheless, a clear anti-bunching signature is still observed in both figures.

7.2 Count rate change

First, to confirm that the SiPMs successfully detect photons emitted from the SPS, we monitored changes in the count rate with bunch of spots and single spot.

Fig 9 shows the time-series plots of the count rates for each condition. In all case, a change in count rate is observed when switching the SPS ON and OFF, indicating that the SiPMs are indeed responding to photons emitted from the SPS. The amount of count rate change(written as SPS rate) is summarized in Table 8.

As expected, the detection rate when the SPS is enabled decreases with the number of spots, as less photons are arriving to the SiPMs. However, as shown in the plots, the photon count attributable to the SPS is significantly smaller than the SiPM's dark count rate. In particular, under the single spot condition, the SPS rate is only around 2-3 kHz, whereas the dark count background remains much higher.

Number of spot	SPS rate in Asic0[Hz]	SPS rate in Asic1 [Hz]
Bunch of spots	1.17×10^4	1.31×10^4
Single spot	2.98×10^3	1.63×10^3

Table 8: The amount of count rate change in each condition with SiPMs

Based on these results, I conducted simulations assuming SPS emission rates of 4 kHz and 15 kHz to estimate the acquisition time required for observing photon anti-bunching. The simulations suggest that more than 60 minutes is needed at 4 kHz, and about 10 minutes at 15 kHz.

7.3 Delay Histogram

Next, I performed long-term data acquisition based on the results of the previous simulations. I began with the bunch-of-spots condition. To avoid errors caused by the blinking behavior (temporal instability) of the nanorods, I divided the measurement into multiple short runs—five acquisitions on different spots of two minutes each, of two minutes each, taken at different spots. The combined result is shown in Fig 10.a).

As shown in Fig 10.a), no clear anti-bunching dip is observed, especially in comparison with the result obtained using SPADs (Fig 8.c).

Subsequently, I extended the measurement time by performing ten acquisitions of two minutes each, totaling 20 minutes. The result is shown in Fig. 10.b). Here, although there is no clear anti-bunching, the tendency can be recognised, suggesting that longer acquisition times significantly improve the visibility of photon correlations when using SiPMs under high-DCR conditions.

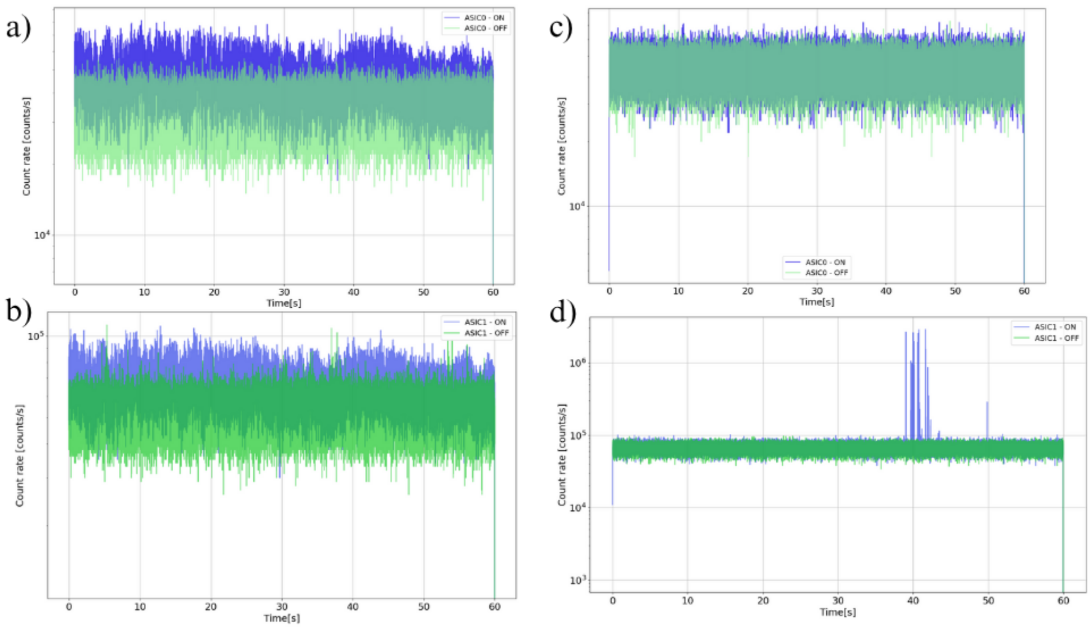

Figure 9: The count rate of each condition with SiPMs. a)The count rate of bunch of spots with SiPM Asic0. b)The count rate of bunch of spots with SiPM Asic1. c)The count rate of single spot with SiPM Asic0. d)The count rate of single spot with SiPM Asic1

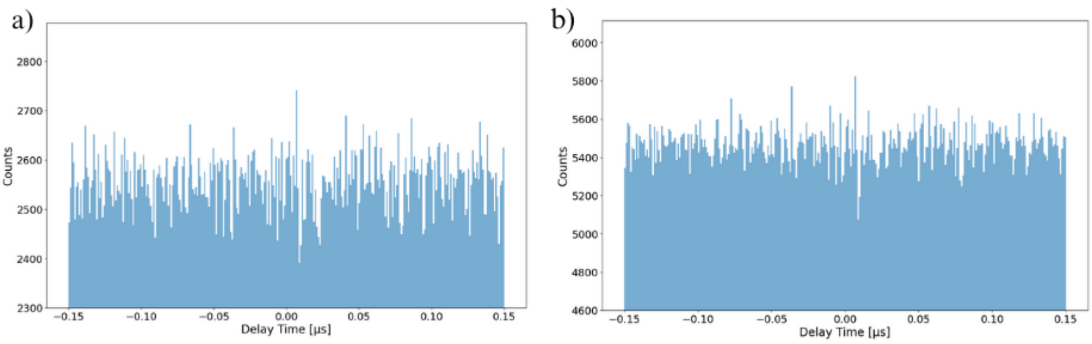

Figure 10: The delay histogram of bunch of spots with SiPMs in a)10 minutes. b)20 minutes

8 Conclusion

The results presented in the previous sections demonstrate that while SiPMs were able to detect changes in photon count rates corresponding to SPS activity, they failed to clearly exhibit photon anti-bunching behavior. This indicates several technical and physical limitations that must be addressed before SiPMs can be reliably used for high-precision single-photon source (SPS) evaluation. There are two main challenges: one experimental and one physical.

(1) Setup alignment and optical coupling efficiency.
Despite the fact that SiPMs have higher photon detection efficiency (PDE) than SPADs, the observed count rates with SiPMs were consistently lower. This suggests a mismatch in optical alignment or coupling efficiency. SPADs used in previous experiments are equipped with integrated micro-lenses or optimized focusing structures, which efficiently guide incoming photons to the active area. In contrast, the bare SiPMs used here may lack such optical enhancement. I attempted various alignment configurations using translation stages and mounts, but only minor improvements were observed. The result implies that further optical engineering, such as introducing lens or fiber-coupling optimization, may be necessary to utilize the full PDE potential of SiPMs in low-photon-flux environments.

(2) High dark count rate (DCR).
A more fundamental limitation is the significantly higher DCR of SiPMs compared to SPADs. In single-photon detection, especially under weak sources like single nanorods, high DCR can hide true photon detection events, degrading the signal-to-noise ratio. As a result, we need to take longer acquisitions to detect anti-bunching. This has two practical problems: (1) more data needs to be stored and analyzed and (2) quantum dots have a limited lifetime, and in the experiments I could observe how their emission was decreasing with time.

In summary, the lack of anti-bunching observation in our SiPM-based setup appears to be caused by first, by a non-efficient optical allignment and, second, duento the limitations imposed by DCR. Nonetheless, our results provide important insights into the practical limitations and considerations for applying SiPMs to precision quantum optical measurements.

Bibliography

[AG19] Fabio Acerbi and Stefan Gundacker. Understanding and simulating sipms. *Nuclear Instruments and Methods in Physics Research Section A: Accelerators, Spectrometers, Detectors and Associated Equipment*, 926:16–35, 2019. Silicon Photomultipliers: Technology, Characterisation and Applications.

[AJW+23] Kanin Aungskunsiri, Sakdinan Jantarachote, Kruawan Wongpanya, Ratthasart Amarit, Pongpun Punpetch, and Sarun Sumriddetchkajorn. Quantum random number generation based on multi-photon detection. *ACS Omega*, 8(38):35085–35092, 2023.

[ASA+20] Zubair Ahmed, Ravinder Singh, Wajahat Ali, Grahame Faulkner, Dominic O'Brien, and Steve Collins. A sipm-based vlc receiver for gigabit communication using ook modulation. *IEEE photonics technology letters*, 32(6):317–320, 2020.

[BB14] Charles H. Bennett and Gilles Brassard. Quantum cryptography: Public key distribution and coin tossing. *Theoretical Computer Science*, 560:7–11, 2014. Theoretical Aspects of Quantum Cryptography – celebrating 30 years of BB84.

[BDB19] Maria Giuseppina Bisogni, Alberto Del Guerra, and Nicola Belcari. Medical applications of silicon photomultipliers. *Nuclear Instruments and Methods in Physics Research Section A: Accelerators, Spectrometers, Detectors and Associated Equipment*, 926:118–128, 2019. Silicon Photomultipliers: Technology, Characterisation and Applications.

[exc20] excelitas. Spcm-aq4c single photon counting module 4 channel array. Technical report, excelitas, 2020.

[Gol23] Alberto Gola. Status and perspectives of sipms at fbk, 2023.

[KE01] Milburn GJ Knill E, Laflamme R. A scheme for efficient quantum computation with linear optics. *Nature*, 409:46–52, Jan 2001.

[MGM+25] D. Mazzanti, Sibila Gómez, J. Mauricio, J. Alozy, F. Bandi, Michael Campbell, Rok Dolenec, Georges Fakhri, José María Fernández-Tenllado Arribas, Alberto Gola, D. Guberman, Stanislaw Majewski, R. Manera, Antonio Mariscal-Castilla, M. Penna, R. Pestotnik, Sara Portero Castillo, A. Paterno, Andreu Sanuy, and David Gascon. Below 100 ps ctr using fastic+, an asic including on-chip digitization for tof-pet and beyond, 06 2025.

[OHM+06] A. N. Otte, J. Hose, R. Mirzoyan, A. Romaszkiewicz, M. Teshima, and A. Thea. A measurement of the photon detection efficiency of silicon photomultipliers. *Nucl. Instrum. Meth. A*, 567:360–363, 2006.

[ons21] onsemi. And9770-d: Introduction to silicon photomultipliers (sipm). Technical Report AND9770-D, onsemi, 2021. Accessed: 2025-07-06.

[RA13] J. Bach et al. R. Agishev, A. Comerón. Lidar with sipm: Some capabilities and limitations in real environment,. *Opt. Laser Technol. 49*, pages 86–90, 2013.

[Sen17] Solomon G. White A. Senellart, P. High-performance semiconductor quantum-dot single-photon sources. *Nature Nanotech 12*, 2017.

A Appendix I: The derivation of the formula for mean number calculation

In this appendix, I derive the formula used to estimate the mean number of detected events per pulse—originating from both photons and dark counts—based on Poisson distribution.

The detection of a single photon by a SiPM is inherently probabilistic. When a large number of laser pulses (e.g., 40,000) are used and the probability of photon detection per pulse is relatively low, the number of detection events per pulse can be modeled by a Poisson distribution:

$$P(k;\lambda) = \frac{\lambda^k e^{-\lambda}}{k!} \tag{7}$$

Here, λ is the mean number of events (photons or dark counts), and k is the number of events observed. In particular, we consider the probability of detecting zero events ($k = 0$), which simplifies to:

$$P_0 = e^{-\lambda} \iff \lambda = N_{ph} = -ln\frac{N_0}{N_{tot}} \tag{8}$$

Where: N_{tot} is the total number of acquisition windows (laser pulses), and N_0 is the number of windows with no detectable signal above a defined threshold. This method has the advantage of being independent of optical crosstalk, since it considers only the no photoelectron detected event.

However, in a real experiment, both photons (when the laser is ON) and dark counts (thermal noise) contribute to detection events. To isolate the effect of actual photons, I performed the same measurement with the laser both ON and OFF.

1. **Laser ON:** Both photons and dark counts contribute
   The mean number of total detections per pulse is:
   $$N_{\mathrm{ph+DC}} = -\ln\left(\frac{N_0^{\mathrm{ON}}}{N_{\mathrm{tot}}}\right) \tag{9}$$
2. **Laser OFF:** Only dark counts contribute
   The mean number of dark count detections per pulse is:
   $$N_{\mathrm{DC}} = -\ln\left(\frac{N_0^{\mathrm{OFF}}}{N_{\mathrm{tot}}}\right) \tag{10}$$

Thus, the mean number of photon-induced detections is:

$$\begin{aligned} N_{\mathrm{ph}} &= N_{\mathrm{ph+DC}} - N_{\mathrm{DC}} \\ &= -\ln\left(\frac{N_0^{\mathrm{ON}}}{N_{\mathrm{tot}}}\right) + \ln\left(\frac{N_0^{\mathrm{OFF}}}{N_{\mathrm{tot}}}\right) \\ &= \ln\left(\frac{N_0^{\mathrm{OFF}}}{N_0^{\mathrm{ON}}}\right) \end{aligned} \tag{11}$$

However, each measured values should have uncertainties. Since N_0^{ON} and N_0^{OFF} are counts following Poisson statistics, and assuming sufficiently large sample sizes, the uncertainties can be approximated using Gaussian statistics:

$$\Delta N_0^{\mathrm{ON}} \approx \sqrt{N_0^{\mathrm{ON}}} \tag{12}$$

$$\Delta N_0^{\mathrm{OFF}} \approx \sqrt{N_0^{\mathrm{OFF}}} \tag{13}$$

Using standard error propagation, the uncertainty in N_{ph} is:

$$\Delta N_{\text{ph}} = \sqrt{\left(\frac{\Delta N_0^{\text{ON}}}{N_0^{\text{ON}}}\right)^2 + \left(\frac{\Delta N_0^{\text{OFF}}}{N_0^{\text{OFF}}}\right)^2} \tag{14}$$

Similarly, the uncertainty in the DCR is derived from:

$$\Delta DCR = \sqrt{\frac{dDCR}{dN_{DC}} * \Delta N_{DC}} \tag{15}$$

$$= \sqrt{\frac{\Delta N_{DC}}{timewindow * 10^{-9}}} \tag{16}$$

This derivation provides the foundation for estimating photon detection rates and their uncertainties under realistic experimental conditions using SiPMs.